Microsc. Microanal. Res. 2022 35(1) 16-20

Microscopy and Microanalysis Research
- The Journal of The Microscopy Society of Thailand

Journal Home Page: https://www.tci-thaijo.org/index.php/mmres/

Microsc. Microanal. Res.

A Microstructural Investigation of PMMA/SAM TiO_2 Dielectric thin Films for OFETs

Kroekchai Inpor[1] Nongluck Houngkamhang[2] Navaphun Kayunkid[2] and Chanchana Thanachayanont[1]

[1] *National Metal and Materials Technology Center, 114, Thailand Science Park, Klong 1, Klong Luang, Pathumthani 12120, Thailand.*
[2] *College of materials innovation and technology, King Mongut's Institute of Technology Ladkrabang, Bangkok 10520, Thailand.*
*Corresponding author's e-mail address: kroekchi@mtec.or.th

ARTICLE INFO

Article history
Submitted: 4 November 2021
Revised: 11 May 2022
Accepted: 13 May 2022
Available online: 24 June 2022

Keywords:
Dielectric constants, PMMA, TiO_2 and Self-assembled monolayer

ABSTRACT

Poly (methyl methacrylate) (PMMA) and TiO_2 were used as dielectric materials of OFETs for improved dielectric constants and better interfaces between the dielectric layers and organic semiconductor films. In this study, PMMA/TiO_2 layers were fabricated using self-assembled monolayer (SAM) TiO_2 films that were inserted between the PMMA film layers. Dielectric constants of the PMMA/TiO_2 layers were studied from capacitance-frequency characteristics of metal/insulator/metal structures. The dielectric constant was found to increase with an increased amount of TiO_2. The dielectric constant at a frequency at 1k was 15.7, which was approximately 4 times higher than that of bare PMMA. However, too high amount of SAM TiO_2 resulted in decreased dielectric constant due to leakage current.

INTRODUCTION

Organic field effect transistors (OFETs) were originally developed by the research group of L. Torsi [1]. OFETs require much less capital investment to manufacture than conventional inorganic Si field effect transistors (FETs). However, performance of the OFETs still needs to be improved. Currently, the amount of bias voltage required for OFETs to operate remains high compared to that required for the Si FETs. According to the structure and working principle of the FETs, charge accumulation in the semiconductor film layers relies on the induction of electric field between gate and source electrodes through an insulating layer in the middle between the gate electrode and the semiconductor layer. Such charge build-up creates a channel between the drain and the sauce electrodes that is directly proportional to the source to drain current (I_{DS}) flowing between them. A large amount of charge accumulation results in a higher I_{DS} flowing between the drain and sauce electrodes. Therefore, one of the key factors for the FETs to achieve high I_{DS} current in low source to gate voltage (V_{GS}) inductance is the high dielectric constant of the insulating layer. The relationship between charge accumulation (N_c) and dielectric constant ($k\varepsilon_0$) is shown in Equation 1 [2].

$$N_c = \frac{k\varepsilon_0}{ed} V_{GS} \quad (1)$$

Where *d* and *e* are thickness of the gate insulator and the charges of an electron, respectively. At present, most substances with high dielectric constants are metal oxides such as TiO_2, SiO_2, etc. Using these materials in OFETs reveals a lot of problems at the interfaces between the organic semiconductors and the metal oxides. In particular, the microscopic surface roughnesses of the materials cause electronic interface trapping at the interfaces. While the use of organic materials as an insulating layer of the OFET is less of a problem, the dielectric constants of organic insulators are too low and result in poor device performance [3]. Combining organic and inorganic insulating materials together has been extensively studied for their combined benefits. Chen et al. mixed TiO_2 nanoparticles into poly-4-vinylphenol (PVP) as a solution and formed dielectric layer thin films for OFETs [4-5]. Majewski et al. fabricated OFETs using a double-layered anodized TiO_2 and poly (α-methylstryrene) (PAMS) as the dielectric layer, with PAMS film in contact with the organic semiconductor layer [6]. Yang et al. fabricated OFETs using a double-layered TiO_2-oleic and PVP as the dielectric layer, with PVP film in contact with the organic semiconductor layer [7,8]. All of them that the efficiency and threshold voltage increased to maximum values and, then, decreased.

In this study, a triple-layered dielectric structure is fabricated with a TiO_2 film layer inserted between the Poly (methyl methacrylate) (PMMA) film layer. Self-assembled monolayer (SAM) technique was used to create the TiO_2 films. The films microstructure was optimized in order to achieve the optimum dielectric constant. The dielectric constants were studied via the capacitance-frequency characteristics of the dielectric layers in the metal-insulator-metal (MIM) structure.

METHODOLOGY

PMMA and titanium dioxide (TiO_2) nanoparticles were purchased from Sigma-Aldrich. MIM devices were fabricated on indium tin oxide (ITO) coated glass substrate (commercial grade) as bottom contacts.

60 mg/ml PMMA solution was dissolved in anisole and fabricated on the ITO substrate by spin coating using 5,500 rpm for 2 minutes in a glovebox. Samples were dried at 75° C overnight in the glovebox. The SAM-TiO_2 nanoparticle films were fabricated by soaking in TiO_2 nanoparticle solution prepared by suspend in deionized water. In the same way of the first layer, the second PMMA films were fabricated on the TiO_2 film. Then, 14x8 mm^2 top contact Aluminum film was deposited by thermal evaporation. These device structures are showed in Figure 1.

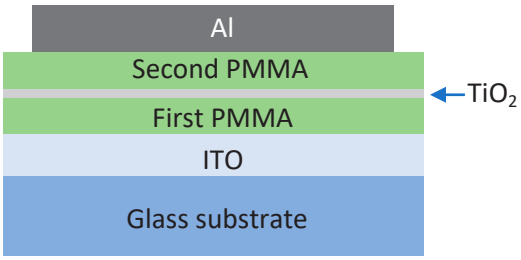

Figure 1. MIM device structure employed in this study.

The crystalline formation of the SAM-TiO_2 in PMMA films was investigated via x-ray diffraction (XRD) (Rigaku, TTRAX III). The film thicknesses were measured by Dektak3030 profilometer. Capacitance versus frequency plots were obtained from an impedance analyzer (Agilent 4294a) with a fixed 10-mV AC voltage. The film surface morphology and roughness were investigated by atomic force microscopy (AFM) (*SEIKO Instruments*, *SPA400*). Transmission electron microscope (JEOL, JEM-2020) and scanning electron microscope (JEOL, JSM-7800F (Prime)) were used to study morphologies of the TiO_2 nanoparticles and interface cross-sections, respectively.

RESULTS AND DISCUSSION

Figure 2 a) shows morphology of the TiO_2 nanoparticles prior to the preparation in deionized water that were analyzed by Transmission Electron Microscopy (TEM). Their shape is ellipsoidal with a diameter of approximately 25x20 nm. Figure 2b) shows a scanning electron microscope (SEM) cross section of a MIM device with the TiO_2 film between the PMMA films. From these two images, the size of TiO_2 in Figure 2b is found to be much smaller than the size of TiO_2 in Figure 2a. Based on the understanding of the SEM process, the different sizes of TiO_2 are due to the low stability of the PMMA film. When an electron beam is emitted to the PMMA film for a long time, it will undergo expansion and flow to obscure the TiO_2 film layer. This caused the size of the TiO_2 film shown in Figure 2b) to be distorted. To confirm the existence of the TiO_2 film, ITO/PMMA/TiO_2/PMMA samples and ITO/PMMA/PMMA samples were analyzed with x-ray diffraction (XRD). From Figure 2, XRD results show differences in x-ray reflectance peak quantities of samples with and without the TiO_2 films. The ITO/PMMA/TiO_2/PMMA peaks indicate both anatase phase and rutile phase of TiO_2 films in two theta angles at 25 and 28 degrees, respectively. These peaks were not found in the ITO/PMMA/PMMA samples. Therefore, this experiment demonstrated that the coating of TiO_2 films by SAM method on PMMA films produced crystalline TiO_2 films. In addition, the peak intensity increased with increased soaking cycles in TiO_2 solution of the SAM fabrication indicating increased crystallinity.

In all results in Figure 4 a) and b), there was a slight decrease in capacitance at low frequencies and a sharp decrease in capacitance until it disappeared at frequencies of around 105 Hz. The reduced capacitance at different frequencies is caused by polarized domains in the insulating layer that cannot move or reposit as the electric field changes with the frequency applied. The reduced capacitance at different

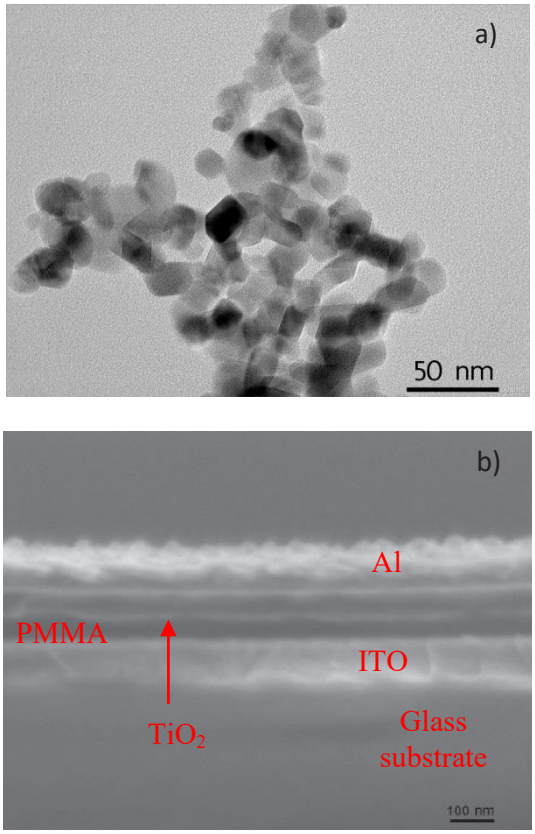

Figure 2. a) A TEM micrograph of TiO_2 nanoparticles and b) a cross-section SEM micrograph (SEM) of ITO/PMMA/TiO_2/PMMA/Al structure on a glass substrate.

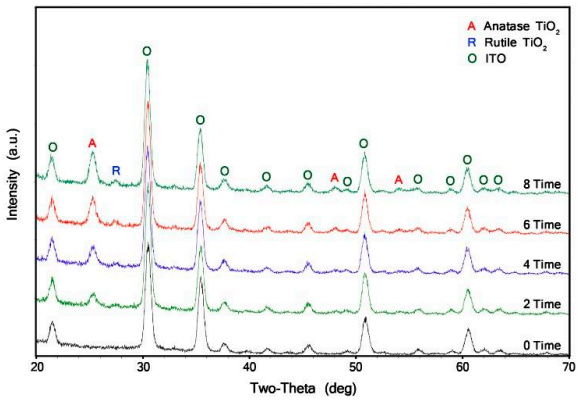

Figure 3. XRD pattern of anatase TiO_2 films on ITO glass substrate/PMMA/TiO_2/PMMA structure with different soaking cycles in TiO_2 solution for SAM fabrication.

frequencies indicates the different polarizing properties of the insulation. From these figure, the initial decrease in capacitance is due to the disappearance of interfacial polarization. This type of polarization is caused by the movement of carrier charges at the grain boundaries within the dielectric substance and the charges accumulated in the defects of the dielectric interfaces with other materials. This decrease in capacitance is due to the inability of the charges to move to the edge of grain boundaries and the contact defects in response to changes of the electric field at higher frequencies applied to the samples. This causes the arrangement of the accumulated charges in the direction of

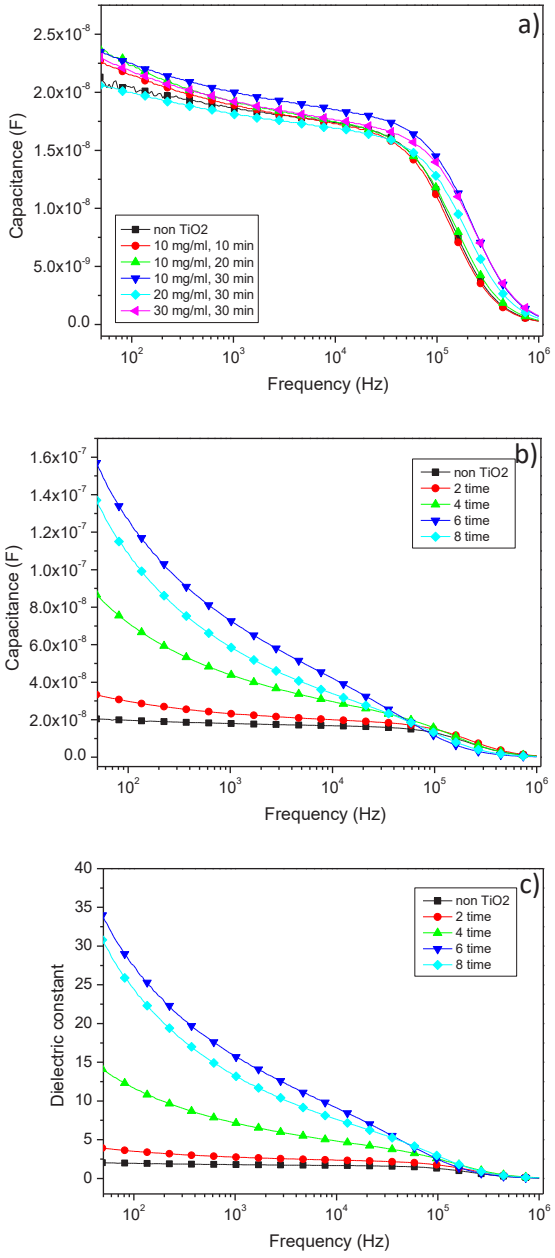

Figure 4. The C-f characteristics of the ITO/PMMA/TiO_2/PMMA/Al device with a) varying concentration and incubation time of SAM TiO_2 onto the structure and b) varying soaking cycles in TiO_2 solution for SAM TiO_2 fabrication and c) ε_r-f characteristics obtained from different soaking cycles in TiO_2 solution for SAM TiO_2 fabrication.

the electric field to decrease, resulting in a decrease in the capacitance value as well [9-11]. The decrease in capacitance at a frequency of about 104 -106 Hz was a reduction from the deterioration of the orientational polarization or dipolar polarization. The absence of this type of polarization is due to the permanently charged dielectric molecules cannot rearrange according to the change in the frequency of the electric field applied. This phenomenon causes a decrease in the charge resulting in a decrease in the capacitance [12]. From the experiment of varying concentration and incubation time of SAM TiO2 onto the structure in Figure 4a, it was found that the change in capacitance of all samples was unclear. These show that the fabrication process cannot change the amount of TiO_2 on the PMMA film. Additionally, this fabrication process was unable to make the TiO_2 content on the PMMA film sufficient to affect the capacitance changes in the MIM devices. The amount of TiO_2 on PMMA film did not increase with the varying concentration and incubation time of SAM TiO_2 which was probably due to property of this technique. This technique was based on different zeta potentials of TiO2 nanoparticles [13] and PMMA films [14]. Although there are many titanium particles on the PMMA film from different concentrations and incubation times of SAM TiO_2, only one layer of titanium particles can be bonded to the PMMA film. Figure 4 b) shows the C-f characteristics of MIM samples modified by different soaking cycles in the TiO_2 solution at a concentration of 10 mg/ml at incubation time for 30 min. It was found that the capacitance was higher with higher soaking cycles in the TiO_2 solution. A relative dielectric constant (ε_r) that was showed in Figure 4 c) can be calculated from the capacitance values in Figure 4 b) and the thickness values of PMMA/TiO_2/PMMA film (see Table 1) by equation 2.

$$\varepsilon_r = \frac{C_i}{C_0} = \frac{\varepsilon_r \varepsilon_{0A}}{dC_0} \quad (2)$$

Where C_0 is the capacitance measured with vacuum between its plates, C_i is the insulator capacitance, ε_0 is the vacuum dielectric constant, A is the area of the capacitor and d is the distance between plates

From previous studies on ε_r of TiO_2, it was found that the ε_r-f characteristics at the low-frequency voltage range was highly related with the film characteristics of TiO_2. The ε_r-f characteristics for the high density TiO_2 films exhibited a constant or slight decrease in ε_r values for the low-frequency voltage range [15-16]. Whereas in samples with low density TiO_2 films exhibited consistent reductions in ε_r values at the low-frequency voltage range [17-18]. These results are related to the theory described in the reduction of ε_r due to interfacial polarization losses at low-frequency voltage ranges. Because in low density TiO_2 films tend to create many grain gaps within the TiO_2 films and many gaps between TiO_2 layers and neighboring films, resulting in a higher ε_r value due to interfacial polarization and a sharp reduction in ε_r – f characteristics at low-frequency voltage ranges. For the SAM experimented in this study, the first layer of TiO_2 nanoparticles on PPMA film is formed by the different zeta potentials of the TiO_2 nanoparticles and the PMMA film. The next layer of TiO_2 recoating is expected to be due to the agglomeration of TiO_2 particles, as this production lacks zeta properties. Therefore, the surface characteristics of the recoated TiO_2 films have increased roughness due to the increased agglomeration of TiO_2 particles. The surface roughness of TiO_2 film on PMMA film was found to increase with increased soaking cycles in TiO_2 solution during the SAM TiO_2 deposition as shown by AFM in Figure 5 and Table 1,

Table 1. Capacitance per unit area (C_i), dielectric constant, thickness, and root mean square (RMS) surface roughness of the ITO/PMMA/TiO_2/PMMA/Al device in different soaking cycles of self-assembled TiO_2 deposition.

Soaking cycles of self-assembled TiO_2 deposition (times)	C_i at 1 kHz (nF/cm²)	Dielectric constant at 1 kHz	Thickness (nm)	RMS surface roughness (nm)
0	16.5	1.78	137	0.4
2	21.3	2.74	164	6.8
4	40.3	7.13	225	20.0
6	66.8	15.7	299	89.3
8	53.8	13.2	311	112.8

respectively. With this TiO_2 film layer fabrication, the additional TiO_2 nanoparticles resulted in an increase of the grain gap within the TiO_2 film as the amount of TiO_2 nanoparticles increased and an increase of the boundary gap between the TiO_2 film and the PMMA film as the agglomeration of the TiO_2 nanoparticle increased. These resulted in an increase in interfacial polarization and a sharp reduction in the ε_r – f characteristics at low-frequency voltage ranges as the soaking cycles of the SAM TiO_2 increased as shown in figure 4c). The reduction of ε_r – f characteristics at 10^4 -10^5 Hz ranges in Figure 4C showed similar curves in all samples. The decrease in ε_r of these frequency range are expected to be mainly due to the dipolar polarization property of PMMA. Furthermore, we found that the ε_r value decreased when more and more SAM TiO_2 nanoparticles were increased. The ε_r of sample with 6 soaking cycles during the SAM TiO_2 deposition was greater than sample with 8 soaking cycles as shown in figure 4c). This is a result of the higher SAM TiO_2 film roughness resulted from more agglomeration, hence, resulting in an increased leakage current.

Table 2 compares the thickness, dielectric constant, and capacitance per unit area of polymer/TiO_2 insulating layer form the best values obtained in this study and previously reported values by others. It was shown that the SAM TiO2 film was inserted between the PMMA film layers yielding the highest ε_r value.

CONCLUSION

In this study, we propose a novel approach to prepare self-assembled monolayered (SAM) TiO2 films between PMMA as an insulating triple-layered dielectric film in organic field effect transistors (OFETs). It was found that the SAM fabrication could increase the amount of TiO_2 nanoparticles from varying the number of soaking cycles and incubation time. The dielectric constant increases with the number of soaking cycles during SAM TiO_2 deposition until a maximum is reached. Then, a charge leakage may occur due to increased TiO_2 agglomeration creating unacceptable roughness of the TiO_2 film surface.

Table 2. Comparisons of the thickness, dielectric constant, and capacitance .per unit area of polymer/TiO_2 insulating layer material

Insulator layer	Thickness (nm)	Dielectric constant	Ci (nF/cm^2)	Reference
PPV/TiO_2	-	11.6	-	[5]
PPV/TiO_2	634	-	10	[7]
PMMA/TiO_2	-	-	11.1	[8]
PMMA/TiO_2	299	15.7	66.8	This work

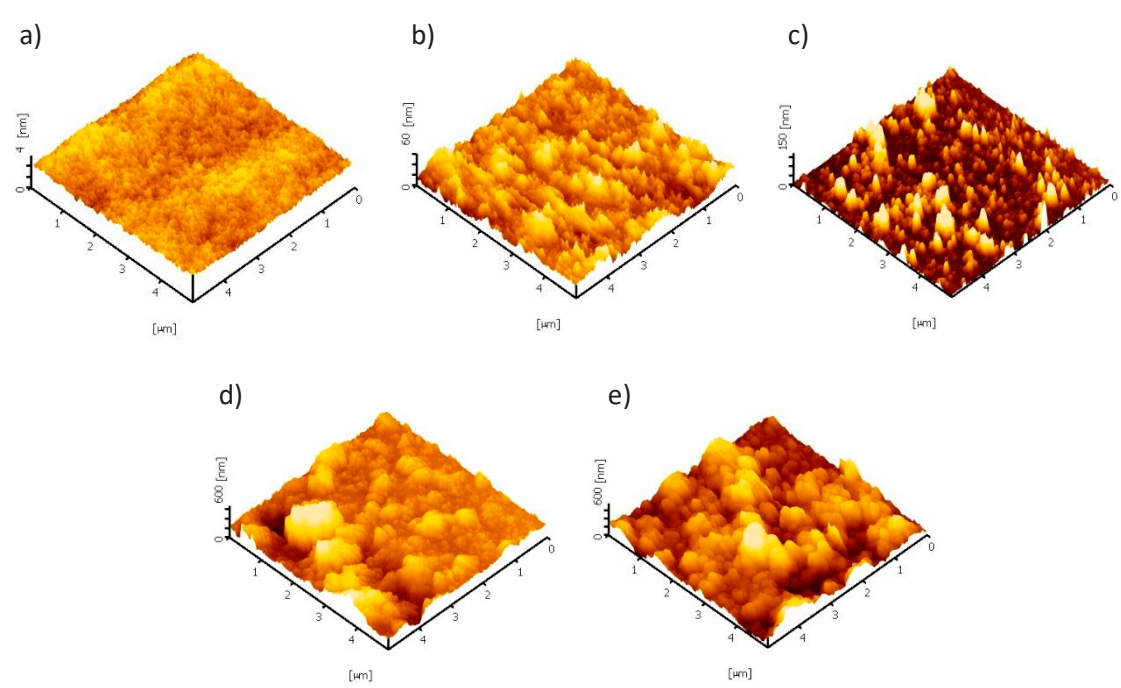

Figure 5. The AFM topographic images obtained from a) PMMA film (without TiO_2) and PTP films prepared by b) 2 soaking cycles, c) 4 soaking cycles, d) 6 soaking cycles and e) 8 soaking cycles in TiO_2 solution.

REFERENCES

[1] Torsi L, Dodabalapur A, Rothberg L J, Fung A W P and Katz H E., Intrinsic transport properties and performance limits of organic field-effect transistors. Seience. 1996 June 7 272;272: 1462-1464.

[2] Wang G, Moses D, Heeger A J, Zhang H, Narasimhan M and Demaray R E., Poly(3-hexylthiophene) field-effect transistors with high dielectric constant gate insulator. Journal of applied physics. 2003 Oct 13;95: 316-322.

[3] Veres J, Ogier S and Lloyd G., Gate insulator in organic field-effect transistors. Chemistry of Materials. 2004 Nov 9;16: 4543-4555.

[4] Chen F, Chu C, He J, Yang, Y and Lin J., Organic thin-film transistors with nanocomposite dielectric gate insulator. Applied Physics Letters. 2004 Oct 11;85: 3295-3297.

[5] Chen F, Chuang C, Lin Y, Kung L, Chen T and Shieh HD., Low-voltage organic thin-film transistors with polymeric nanocomposite dielectrics. Organic Electronics. 2006 July 21;7: 435-439.

[6] Majewski LA, Schroeder R and Grell M., Low-voltage, high-performance organic field-effect transistors with an ultra-thin TiO_2 layer as gate insulator. Advanced functional materials. 2005 May 27;15: 1017-1022.

[7] Yang F, Chang K, Hsu M and Liu C., Low-operative-voltage polymer transistor with solution processed low-k polymer/high-k metal-oxide bilayer insulators. Organic Electronics. 2008 June 18;9: 925-929.

[8] Yang F, Hsu M, Hwang G and Chang K., High-performance poly(3-hexylthiophene) top-gate transistors incoporating TiO2 nanocomposite dielectrics. Organic Electronics. 2010 Oct 13;11: 81-88.

[9] Wypych A, Bobowska I, Tracz M, Opasinska A, Kadlubowski S, Krzywania-Kaliszewska A, Grobelny J and Wojciechowski P., Dielectric properties and characterization of titanium dioxide obtained by different chemistry methods. Journal of Nanomaterials. 2014 March 19;2014: Article ID 124814.

[10] Feng Y, Yin J, Chen M, Song M, Su B and Lei Q., Effect of nano-TiO_2 on the polarization process of polyimide-TiO_2 composites. Materials Letters. 2013 Jan 22;96: 113-116.

[11] Abouelhassan S., Investigation of the dielectric properties and thermodynamic parameters of (50- x) P_2O_5 -xAgI -40Ag_2O -10Fe_2O_3 ionic glass. Chinese journal of physics. 2008 Dec 28;48: 650-661.

[12] Harun M H, Saion E, Kassim A, Mahmud E, Hussain M Y and Mustafa I S., Dielectric Properties of Poly (vinyl alcohol)/ Polypyrrole Composite Polymer Films. Journal for the advancement of science & arts. 2009 Jan-June;1: 9-16.

[13] Suttiponparnit K, Jiang J, Sahu M, Suvachittanont S, Charinpanitkul T and Biswas P., Role of Surface Area, Primary Particle Size, and Crystal Phase on Titanium Dioxide Nanoparticle Dispersion Properties. Nanoscale research letters. 2010 Sep 3;2011:

[14] Falahatl H. Wong L, Davarpanah L, Garg A, Schmltz P and Barz D P J., The zeta potential of PMMA in contact with electrolytes of various conditions: Theoretical and experimental investigation. Electrophoresis. 2013 Nov 11;35: 870-882.

[15] Berberich L J and Bell M E., The dielectric properties of the Rutile form of TiO2. Journal of applied physics. 1940 June 13;11: 681-692.

[16] Mardare D and Rusu G., Comparison of the dielectric properties for doped and undoped TiO_2 thin films. Journal of Optoelectronics and Advanced Materials. 2004 March;6: 333-336.

[17] Hu W, Li L, Tong W and Li G., Supersaturated spontaneous nucleation to TiO_2 microspheres: synthesis and giant dielectric performance. Chemical communications journal. 2010 April 9;46: 3113-3115.

[18] Asiah M N, Mamat M H, Khusaimi Z, Abdullah S and Rusop M., Dielectric properties of bulk TiO_2 nanowires prepared by hydrothermal method. The *2012 IEEE Symposium on Business, Engineering and Industrial Applications*. 50-52.